The Step-Mountain Eta Coordinate Model: Further Developments of the Convection, Viscous Sublayer, and Turbulence Closure Schemes

ZAVIŠA I. JANJIĆ*

University Corporation for Atmospheric Research, National Meteorological Center, Washington, D.C.

(Manuscript received 12 March 1993, in final form 9 August 1993)

ABSTRACT

The step-mountain eta model has shown a surprising skill in forecasting severe storms. Much of the credit for this should be given to the Betts and Miller (hereafter referred to as BM) convection scheme and the Mellor–Yamada (hereafter referred to as MY) planetary boundary layer (PBL) formulation. However, the eta model was occasionally producing heavy spurious precipitation over warm water, as well as widely spread light precipitation over oceans. In addition, the convective forcing, particularly the shallow one, could lead to negative entropy changes.

As the possible causes of the problems, the convection scheme, the processes at the air–water interface, and the MY level 2 and level 2.5 PBL schemes were reexamined. A major revision of the BM scheme was made, a new marine viscous sublayer scheme was designed, and the MY schemes were retuned.

The deep convective regimes are postulated to be characterized by a parameter called "cloud efficiency." The relaxation time is extended for low cloud efficiencies, and vice versa. It is also postulated that there is a range of reference equilibrium states. The specific reference state is chosen depending on the cloud efficiency. The treatment of the shallow cloud tops was modified, and the shallow reference humidity profiles are specified requiring that the entropy change be nonnegative.

Over the oceans there are two layers: (a) a viscous sublayer with the vertical transports determined by the molecular diffusion, and (b) a layer above it with the vertical transports determined by the turbulence. The viscous sublayer operates in different regimes depending on the roughness Reynolds number.

The MY level 2.5 turbulent kinetic energy (TKE) is initialized from above in the PBL, so that excessive TKE is dissipated at most places during the PBL spinup. The method for calculating the MY level 2.5 master length scale was rectified.

To demonstrate the effects of the new schemes for the deep convection and the viscous sublayer, tests were made using two summer cases: one with heavy spurious precipitation, and another with a successful 36-h forecast of a tropical storm. The new schemes had dramatic positive impacts on the case with the spurious precipitation. The results were also favorable in the tropical storm case.

The developments presented here were incorporated into the eta model in 1990. The details of further research will be reported elsewhere. The eta model became operational at the National Meteorological Center, Washington, D.C., in June 1993.

1. Introduction

Mesinger (1984) proposed the so-called eta coordinate using a steplike mountain representation (see also Mesinger and Janjić 1984, 1985, 1987). In contrast to the sigma coordinate (Phillips 1957), the eta coordinate surfaces are quasi-horizontal everywhere. At the same time the simplicity of the sigma system lower boundary condition is preserved.

With the eta coordinate, three major problems can be anticipated: (a) the internal boundaries at the vertical sides of the mountain walls, (b) the code optimization, and (c) the physical package. The first two were discussed by Mesinger et al. (1988). They implemented the eta coordinate in the "minimum physics," sigma coordinate HIBU (Hydrometeorological Institute and Belgrade University) limited-area model. This model will be referred to as the "eta model." The eta model is defined on the semistaggered Arakawa E grid (e.g., Mesinger and Arakawa 1976) and uses the technique for preventing grid separation (Mesinger 1973; Janjić 1974, 1979; Vasiljević 1982) in combination with split-explicit time differencing (Mesinger 1974; Janjić 1979). The horizontal advection used in the model has a built-in strict nonlinear energy cascade control (Janjić 1984a,b; Janjić and Mesinger 1984).

The problem of the physical package was addressed by Janjić (1990) (see also Janjić 1988a; Janjić et al. 1988a; Janjić et al. 1988b). The package was based on

* Current affiliation: Department of Meteorology, College of Physics, University of Belgrade, Belgrade, Yugoslavia.

Corresponding author address: Prof. Zaviša I. Janjić, Department of Meteorology, College of Physics, University of Belgrade, P.O. Box 550, YU-11001 Belgrade, Yugoslavia.

the Mellor–Yamada level 2.5 scheme (Mellor and Yamada 1974, 1982), the Mellor–Yamada level 2 scheme for the "surface" layer (Mellor and Yamada 1974, 1982) with a dynamical turbulence layer several meters deep at the bottom, surface processes designed following Miyakoda and Sirutis (1977, 1983) and Miyakoda et al. (1986), fourth-order lateral diffusion with the diffusion coefficient depending on the deformation (cf. Smagorinsky 1963; Miyakoda and Sirutis 1977, 1983; Miyakoda et al. 1986) and the turbulent kinetic energy (TKE) (cf. Lilly 1962; Xu 1988), conventional large-scale precipitation with evaporation, slightly modified deep and shallow convection schemes proposed by Betts (1986) and Betts and Miller (1986, hereafter referred to as the BM scheme or the BM formulation), and the National Meteorological Center (NMC) version of the Goddard Laboratory for Atmospheres (GLA) radiation scheme (Davies 1982; Harshvardhan and Corsetti 1984). For additional details on the eta model the reader is referred to the documentation prepared by Black (1988), Gerrity and Black (1987), and Lazić and Telenta (1990).

The most comprehensive testing, tuning, and further development of the model have been carried out at NMC, Washington, D.C. With varying resolutions and integration domain sizes, the eta model has also been implemented in the tropics (Lazić 1990, 1993a,b; Lazić and Telenta 1990; Rogers et al. 1991), over Europe (e.g., Janjić and Lazić 1988), as well as in many other geographical areas all over the world. An interesting feature of the model is that little retuning is needed when the horizontal resolution is changed. As a matter of curiosity, the model was successfully run even with 4-km grid spacing in a realistic simulation of a precipitation event over Sicily (S. Ničković 1993, personal communication).

The "standard" resolution used in most runs was 80 km in the horizontal and 16 layers in the vertical. The model atmosphere extended up to 100 hPa. The depths of the layers slowly increased from the ground up to the middle of the atmosphere and then decreased as the top of the model atmosphere was approached. The "standard" integration domain covered the North American continent and the adjacent waters. For this region, the NMC products were used in order to specify the initial and the boundary conditions, as well as for the verification. As a robust, quick-response tool, the model with the standard resolution and the standard integration domain was also used for the experiments discussed in this paper.

Note that increased resolution and approximately equidistant eta coordinate surfaces are needed in the lower troposphere in order to resolve the mountains well and to treat the interaction between the atmosphere and the underlying surface approximately equally well over both low-lying and elevated terrain. Applying this principle with the standard vertical resolution, the height of the lowest model level above the underlying surface—that is, the depth of the model "surface layer"—was about 150 m, and accordingly, the depth of the lowest model layer was about 300 m.

Black and Mesinger (1989), Mesinger and Black (1989), and Mesinger et al. (1990) reported on further improvements of the model. Among these, the scheme for the vertical advection of moisture was replaced by a schéme based on the piecewise linear method (PLM) approach (Carpenter et al. 1990), and the viscous interfacial sublayer between the surface and the atmosphere was added. In addition, the convection scheme was revised and retuned in cooperation with Betts. Finally, due to technical reasons the GLA radiation package was replaced by the Geophysical Fluid Dynamics Laboratory (GFDL) scheme.

The results of the tests carried out at NMC were presented by Black and Janjić (1988), Black and Mesinger (1989, 1991), Black et al. (1989, 1990), Mesinger and Black (1989, 1991), Mesinger et al. (1990), Rogers et al. (1991), and Ward (1990). In most of these studies, special attention was paid to precipitation as an important prognostic variable, which is perhaps most difficult to predict accurately. In the periods considered, the eta model generally had a considerable advantage over the operational NMC regional precipitation forecasts produced by a sophisticated model with comparable resolution over North America and adjacent waters and requiring about the same computational effort. Concerning the synoptic features, an overall impression was that the main advantage of the eta model over the operational NMC regional forecasting system were improved predictions of major storm systems (e.g., WGNE 1989, 1990).

In the tropics the model was tested in 48-h simulations of the tropical cyclones from the Australian Monsoon Experiment (AMEX) period (Lazić and Telenta 1990; Lazić 1990, 1993a,b). From the synoptic point of view, the results were considered as remarkably good, both in absolute terms and compared to the results obtained with other models (Lazić and Telenta 1990; Lazić 1990, 1993a,b). In the NMC quasi-operational and experimental runs the model also showed a surprising skill in forecasting the development, deepening, and subsequent movement of tropical storms in the warm part of the year (e.g., Black et al. 1989; Mesinger et al. 1990; Ward 1990; Rogers et al. 1991).

Undoubtedly, much of the credit for the successful forecasts of the precipitation and the storm systems should be given to the BM convection scheme and the planetary boundary layer (PBL) formulation. However, the tests revealed that on some occasions the model tended to produce heavy spurious precipitation, particularly over warm water. Although the precipitation over the oceans could not be verified due to the lack of observations, indirect evidence, such as developments of spurious lows, suggested that the precipitation was too heavy.

This problem has been known for some time, and the aforementioned modification of the vertical advection of moisture, the reformulation and retuning of the convection scheme, and the introduction of the viscous sublayer were actually aimed at coping with it. Although significant improvement was achieved, the occasional heavy spurious precipitation would not go away, impairing severely the forecasts when it showed up in full strength. Another problem that the eta model shared with many other models was widely spread excessive light precipitation over water.

Both problems could be dealt with by an ad hoc technique for reducing the surface fluxes. It was felt, however, that an indiscriminate reduction of the fluxes could impair the ability of the model to handle the severe storms. To examine the problems involved and to test the techniques developed, two extreme summer cases were chosen. In the case starting at 0000 UTC 20 July 1989, an unsuccessful 48-h forecast with heavy spurious precipitation was obtained. In contrast to that, in the case of 0000 UTC 31 July 1989, the version of the model run quasi-operationally at NMC produced a successful 36-h forecast of the Tropical Storm Chantal (Black et al. 1989).

2. Excessive precipitation and other problems

a. Heavy spurious precipitation

In the case of 20 July, a single grid point was selected for a closer inspection in the middle of a heavy spurious convective precipitation area in the Gulf of Mexico. At this point a strong instability existed in the surface layer even in the initial data. The difference between the virtual potential temperatures at the top of the surface layer and the sea surface was −2.52°C. As can be inferred from the example shown in Fig. 1, later on in the forecast the perpetuation of the instability seems to have been assisted, if not caused, by the deep convection. In the figure, the model temperature profile is shown (diamonds connected by solid line) after 505 time steps, or about 34 h of forecast time, together with the BM reference profile in the previous call of the convection subroutine (squares connected by the solid line). As can be seen from the figure, the convection scheme produces a strong cooling at the cloud bottom (model level 15) and quite modest warming at upper levels. The PBL schemes respond by producing large exchange coefficients trying to remove the instability. In the surface layer, the Mellor–Yamada level 2 exchange coefficients for heat (and moisture) and momentum [cf. Janjić 1990, Eqs. (4.6) and (4.7)] were $K_{H\text{sfc}} = 22\ \text{m}^2\ \text{s}^{-1}$ and $K_{M\text{sfc}} = 17\ \text{m}^2\ \text{s}^{-1}$, respectively. At the top of the lowest model layer (the interface of the model layers 15 and 16), TKE and the Mellor–Yamada level 2.5 heat (and moisture) and momentum exchange coefficients [cf. Janjić, 1990, Eqs. (3.4)] reached $q^2_{1516}/2 = 0.2\ \text{m}^2\ \text{s}^{-2}$, $K_{H^{1516}} = 89\ \text{m}^2\ \text{s}^{-1}$, and $K_{M^{1516}} = 36\ \text{m}^2\ \text{s}^{-1}$, respectively. As a result, the heat and moisture were transferred upward, warming (and moistening) the cloud bottom and at the same time cooling (and drying) the subcloud layer, thereby increasing the instability of the surface layer. In the next call of the convection, the cloud bottom is cooled and dried again.

b. The deep convection scheme over water: Diagnostics and sensitivity tests

The performance of the deep convection scheme over water is especially interesting because a virtually unlimited supply of latent and sensible heat is available. In the present study, the "entropy change"

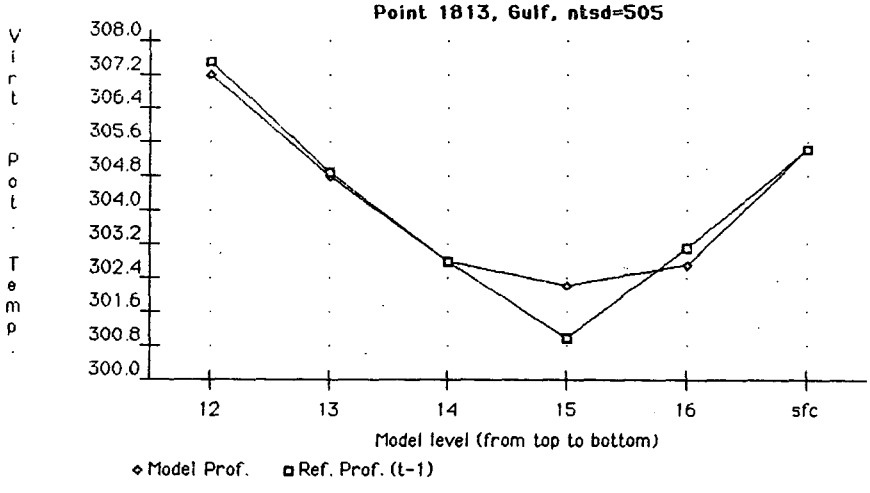

FIG. 1. The temperature profile at a point with heavy convective precipitation (diamonds) after 505 time steps, or about 34 h of forecast time, and the convective temperature reference profile in the previous call of the convection subroutine (squares).

$$\Delta S = \sum \left(\frac{c_p \Delta T + L_{wv} \Delta q}{T} \right) \Delta p \qquad (2.1)$$

was introduced as a diagnostic quantity. Here, the summation is performed from the cloud top to the cloud bottom, Δp are the depths of the model layers in terms of pressure, and c_p and L_{wv} are the specific heat at constant pressure and the latent heat of the water vapor transition, respectively. The symbols ΔT and Δq denote the changes of temperature and specific humidity within a convection time step Δt; that is,

$$\Delta T = (T_{ref} - T^n) \frac{\Delta t}{\tau},$$

$$\Delta q = (q_{ref} - q^n) \frac{\Delta t}{\tau}. \qquad (2.2)$$

In (2.2) the subscript ref indicates the equilibrium reference profiles (Betts 1986), the superscripts n denote the values of temperature and specific humidity at the model levels at the beginning of the time step, and τ is a constant relaxation time (Betts 1986). The temperature T appearing in the denominator of (2.1) is defined as the mean over the time step; that is,

$$T = T^n + \frac{\Delta T}{2}. \qquad (2.3)$$

At the chosen steady convective point over the sea, the entropy change (2.1) was decreasing with time eventually approaching zero, while the precipitation ΔP_B produced in a time step was increasing. The ratio of $\Delta S / \Delta P_B$ was about 50 times larger at the beginning than at the end of a 48-h forecast. This may be viewed as a process that in the limit approaches an adiabatic regime resembling that of the large-scale precipitation, except for the fact that the precipitation occurs at much lower threshold values of relative humidity. In addition, on rare occasions, nonzero precipitation was observed accompanied by a negative entropy change. In such cases the deep convection was aborted, similarly as in the case of the negative precipitation (Betts 1986).

The sensitivity tests revealed that suppressing the deep convection had a generally positive impact on the spurious precipitation. For example:

(i) Increasing the relaxation time τ, the amount of the spurious precipitation could be considerably reduced in the case of 20 July. However, in some other cases, overextending the relaxation time led to the replacement of the heavy spurious convective precipitation by the heavy spurious large-scale precipitation.

(ii) The scheme showed sensitivity to restrictions with respect to the stability of the reference profiles, primarily at higher levels.

(iii) Sensitivity was also detected in the distribution of the precipitation between the convection and the large-scale precipitation (controlled by the threshold relative humidity for the onset of the large-scale precipitation). Typically, the more precipitation is produced by the large-scale precipitation the better.

(iv) There was a positive impact of switching off the convection when the large-scale precipitation starts.

(v) Finally, a somewhat less well-defined sensitivity was found to the specification of the reference cloud bottom and freezing-level humidity.

However, none of the listed devices, separately or combined, proved to be capable of eliminating or sufficiently reducing the spurious precipitation and at the same time preserving to an acceptable extent the skill of the model in forecasting strong convectively driven circulations.

c. *The shallow convection scheme problems*

A rather disturbing feature of the BM shallow convection scheme was first discovered in the NMC medium-range forecasting system. It was noticed that the shallow convection may transport both moisture and heat downward (M. Iredell 1989, personal communication). The early response to the problem was just to abort the convection if the reference profile is less stable than the model profile.

The entropy change test introduced later in the eta model revealed that on many occasions the shallow convection was associated with decreasing entropy. This was particularly the case at the points where the deep convection algorithm was replaced by the shallow one because of negative precipitation (Betts 1986). In the BM scheme jargon, such points are called swap points. The number of points passing the test increased when the modification above the cloud top introduced to represent the inversion (Betts 1986) was excluded from the entropy change calculation.

d. *Identification of possible problem areas*

Concerning the excessive precipitation, two most likely scenarios emerge as candidates for closer inspection.

1) The spurious convection fuels itself by creating too strong thermal instability below the cloud bottom and thus forcing the PBL schemes to transport too much heat and moisture from the underlying ocean surface.

2) There is a physical mechanism limiting the vertical turbulent fluxes, but the PBL schemes fail to reproduce this mechanism properly, so that excessive heat and moisture are supplied to the convective column.

Evidence was accumulating suggesting that instead of retuning and/or minor modifications, a more substantial revision of the convection scheme might be desirable. The ad hoc techniques tested in section 2b failed to eliminate or sufficiently reduce the spurious precipitation and at the same time preserve the ability

of the model to forecast strong convectively driven circulations. The negative entropy changes, associated particularly with the shallow convection, could hardly be considered acceptable in a process that was assumed to be thermodynamically driven. The arbitrariness of the shallow cloud top specification at the swap points (Betts 1986) was another unattractive feature of the scheme.

On the other hand, the PBL could not be accused of all the difficulties. If a layer of air is kept at a constant temperature and humidity at the bottom and constantly cooled and dried at the top, the PBL schemes respond by producing large turbulent fluxes trying to remove the superadiabatic (in terms of the virtual potential temperature) lapse rates. One should recall that in many situations the ability of the PBL to generate large turbulent fluxes leads to spectacular forecasts of strong convectively driven circulations. Nevertheless, the question whether and under what conditions the turbulent fluxes can be overestimated by the PBL certainly requires careful examination. This applies also to the viscous sublayer at the air–water interface.

Thus, the following three major areas requiring closer examination were identified:

1) the deep and shallow convection schemes,
2) the processes at the interface between the sea and the air (the viscous sublayer), and
3) the Mellor–Yamada level 2.5 and level 2 turbulence schemes used above the surface layer and in the surface layer, respectively.

3. Revised convection scheme

a. Deep convection

Within the BM concept, the deep convection is viewed as a thermodynamically driven process that transports the heat and moisture upward in order to remove or reduce the conditional instability. The precipitation is produced in the process. These vertical transports of heat and moisture will be called "convective mixing" or just "mixing." The entropy change ΔS defined by (2.1) will be used as the measure of the intensity of the mixing. Note that with total enthalpy of a column unchanged, a negative change of enthalpy at lower levels and a positive one at higher levels result in a positive entropy change since the temperature is generally decreasing with height.

With the revised scheme the concept of the convection as a process of basically thermodynamic nature is retained. As already discussed in the preceding section, the convective columns over the sea, which eventually develop heavy precipitation, evolve through a range of convective regimes. One of the basic postulates of the revised scheme is that the basic features of these regimes can be characterized by a parameter that will be called "cloud efficiency." This parameter is defined by

$$E = \text{const}_1 \frac{\bar{T}\Delta S}{c_p \sum \Delta T \Delta p}. \tag{3.1}$$

Here, const_1 is a nondimensional constant and $\bar{T}$ is the mean temperature of the cloud

$$\bar{T} = \frac{\sum (T^n + \Delta T/2)\Delta p}{p_{\text{bot}} - p_{\text{top}}}, \tag{3.2}$$

where the subscripts bot and top denote the values at the cloud bottom and at the cloud top. The expression appearing in the denominator of (3.1),

$$c_p \sum \Delta T \Delta p = \frac{\Delta P_B}{\text{const}_2}, \tag{3.3}$$

is proportional to the single time-step precipitation ΔP_B as defined in the BM formulation. As can be seen from (3.1)–(3.3), the cloud efficiency is proportional to the mean cloud temperature and the entropy change and inversely proportional to the BM single time-step precipitation. It does not depend on the ratio of Δt and τ, except through the mean temperatures in (2.3) and (3.2). This dependence can be disregarded since the temperature changes $\Delta T/2$ are two to three orders of magnitude smaller than the temperatures T^n. Alternatively, T in (2.3) and (3.2) could be replaced by T^n, but as can be easily verified, the impact of this modification would be negligible. Note that E is a nondimensional parameter. The efficiency it measures is the ability of the convective column to transport the enthalpy upward and at the same time produce as little precipitation as possible.

With the experience reported in the preceding section, it seems natural to relate the convective regime defined by the cloud efficiency with the convective forcing. Thus, an assumption is made that the convective forcing is proportional to an increasing function of the cloud efficiency $F(E)$; that is, starting from (2.2),

$$\Delta T = (T_{\text{ref}} - T^n)\frac{\Delta t F(E)}{\tau},$$

$$\Delta q = (q_{\text{ref}} - q^n)\frac{\Delta t F(E)}{\tau}, \tag{3.4}$$

or

$$\Delta T = (T_{\text{ref}} - T^n)\frac{\Delta t}{\tau/F(E)},$$

$$\Delta q = (q_{\text{ref}} - q^n)\frac{\Delta t}{\tau/F(E)}, \tag{3.5}$$

As can be seen from (3.5), the modification (3.4) can be interpreted as a new definition of the relaxation time

$$\tau_1 = \frac{\tau}{F(E)}, \tag{3.6}$$

where τ is a constant as before. Note that the relaxation time (3.6) is increasing with decreasing cloud efficiency,

and vice versa. Depending on the relaxation time, the convective regimes will be considered "fast" or "slow."

With the new definition of the relaxation time, the single time-step precipitation takes the form

$$\Delta P = \Delta P_B F(E), \tag{3.7}$$

or

$$\Delta P = \text{const}_2[\sum c_p(T_{\text{ref}} - T^n)\Delta p]\frac{\Delta t}{\tau_1}. \tag{3.8}$$

Recalling point (i) of section 2b, the decision to define F as an increasing function of E seems to be a step in the right direction. In this way, the heavy precipitation is slowed down in the case of the low cloud efficiency, which appeared beneficial in some cases. Concerning the form of the function F, with the present knowledge one has little choice but to use the first-order approximation, that is, to assume it to be linear. Note that the formulas (3.4)–(3.8) are identical to the standard BM formulas for $F = 1$.

As the major deviation from the original concept of the BM scheme, it is further postulated that there is no single convective equilibrium state but rather a range of equilibrium states toward which the column should be forced in the course of its convective history. In this regard two fundamental questions arise.

1) What are the characteristics of various convective equilibrium states, and how should they be represented in the parameterization scheme?

2) What are the large-scale parameters, if any, controlling the transition from one regime to another?

The temperature profiles proposed by Betts (1986) seem to be a rather steady feature of the deep moist convection. In contrast to that, as can be inferred from the Betts (1986) data, the observed humidity profiles are more variable. Thus, it is assumed that the humidity profiles are the main identifying features of the different convective equilibrium states.

As in the BM formulation, constructing the first-guess reference profiles, the moisture is expressed in terms of

$$\text{dsp} = p_{\text{sat}} - p,$$

where p is pressure at a model level and p_{sat} is the saturation pressure in the dry-adiabatic ascent starting from that level. Concerning the choice of the parameter controlling the transition between the equilibrium moisture profiles, it is again assumed to be the cloud efficiency; that is,

$$\text{dsp}^1_{\text{ref}}(p) = G(p, E).$$

Here, the superscript 1 followed by the subscript ref denotes the first-guess reference profile. To incorporate this assumption into the parameterization scheme, two extreme $\text{dsp}^1_{\text{ref}}$ profiles are defined, corresponding, respectively, to (a) a drier, faster (in the sense of the relaxation time), predominantly mixing stage with high cloud efficiency and to (b) a mature, moister and slower (in the sense of the relaxation time), predominantly rainmaking stage with low cloud efficiency. In each time step, the equilibrium $\text{dsp}^1_{\text{ref}}$'s are assumed to be defined in between these two profiles by the function $G(p, E)$. Concerning the form of function G, from what has been said, $\text{dsp}^1_{\text{ref}}$'s should be decreasing with increasing cloud efficiency, and as in the case of the function F, one has little choice but to assume G to be linear. As in the BM formulation, the final reference profiles are constructed by requiring that the enthalpy of the equilibrium reference state be the same as that of the model.

In practice, the constant const_1 appearing in the definition of the cloud efficiency (3.1) is estimated experimentally. The value that has been used for some time in the eta model is $\text{const}_1 = 5$. Also, an upper and a lower limit are imposed on E; that is, $E_1 < E < E_2$. With the chosen value of const_1, E_2 is set to 1, and the lower limit $E_1 = 0.20$ is determined empirically. In addition, in order to prevent the two-grid-interval oscillation in time, the cloud efficiency used in the actual calculations is defined as

$$E^n = \frac{aE^{n*} + bE^{n-1}}{2}, \quad a + b = 1, \tag{3.9}$$

where E^{n*} is given by (3.1). The values chosen are $a = b = 0.50$.

The function $F(E)$ is defined by

$$F(E) = F_1 + (E - E_1)\left(\frac{F_2 - F_1}{E_2 - E_1}\right),$$

where E is obtained from (3.9). The experimentally determined extreme values $F_1 = 0.70$ and $F_2 = 1$ correspond to the extreme values of the cloud efficiency E_1 and E_2. For example, with these values, for the minimum cloud efficiency E_1 the equivalent relaxation time (3.6) increases to $\tau_1 = 4285$ s compared to 3000 s corresponding to the maximum cloud efficiency E_2.

Similarly,

$$\text{dsp}^1_{\text{ref}}(p) = \text{dsp}^1_{\text{ref}^1}(p) + (E - E_1) \times \left[\frac{\text{dsp}^1_{\text{ref}^2}(p) - \text{dsp}^1_{\text{ref}^1}(p)}{E_2 - E_1}\right].$$

As before, the subscripts 1 and 2 represent the two extreme profiles, E is the cloud efficiency, and the superscript 1 followed by the subscript ref denotes the first-guess reference variables. However, since the $\text{dsp}^1_{\text{ref}}$'s have to be defined before the final reference profiles are constructed, the cloud efficiency from the previous time step, that is, E^{n-1}, is used in the above formula. The vigorous mixing stage is assumed to be characterized by relatively dry profiles, while a moister profile is used for the "decaying," rain-making stage approaching the pseudoadiabatic large-scale precipi-

tation process. In the case of the extreme fast (in the sense of the relaxation time) equilibrium profile, at the three characteristic levels of the BM scheme, the cloud bottom, the freezing level, and the cloud top, dsp^1_{ref2}'s are -38.75, -58.75, and -18.75 hPa, respectively. For the extreme slow (in the sense of the relaxation time) equilibrium humidity profile, the dsp^1_{ref1}'s are proportional to those for the fast profile, where the factor of proportionality is of the order of $F_S = 0.60$.

If negative precipitation is encountered, the deep convection is aborted and the shallow convection is attempted (the swap is performed). The same is done in the case of the negative entropy change, even if the precipitation is positive.

In the tests a considerable sensitivity was found with respect to the choice of the humidity profiles and the lower limit for the cloud efficiency. Generally, moister slow profiles are more effective in reducing the convective precipitation and turn it earlier into the large-scale precipitation. The reduction of the convective precipitation can be explained by increased storage of water in the column and the reduced gradient of the specific humidity between the cloud bottom and the level below. In addition to the increased equilibrium state humidity in the column, a smooth transition to the large-scale precipitation is presumably further facilitated by the extended relaxation time that allows the column to reach the threshold value for the onset of the large-scale precipitation earlier.

Early attempts to apply a unified convection scheme for both sea and land resulted in a slight degradation of the precipitation scores over land. Since the situation was not clear, at that time no modification of the BM scheme was made over land.

b. *Shallow convection*

As in the case of the deep convection, a number of modifications have been introduced into the shallow convection scheme. Instead of prescribing arbitrary cloud tops at the swap points, the shallow cloud tops are identified by the jump in the relative humidity (as suggested by Betts). This procedure is extended also to the regular shallow convection points in order to use everywhere the same parameterization scheme for the same physical process. Note that the stability change could also be used for defining the cloud tops.

Shifting the cloud top one level up and applying the special technique for defining the first-guess reference values of temperature and moisture in order to represent the inversion (Betts 1986) was abandoned. The clouds with enhanced and modified cloud tops failed the entropy change test much too often.

Except for the level above the cloud, the first-guess temperature profile is again obtained following the BM formulation. Since the precipitation is not allowed, as before, the final reference profiles are obtained enforcing separately the enthalpy conservation for T and q (Betts 1986). Thus, the final reference profile for temperature can be constructed independently from the humidity profile.

The major deviation from the BM scheme is again the procedure used for constructing the reference humidity profiles. Closer inspection of the Betts (1986) data reveals that the humidity profiles depend on the stability of the temperature profiles. Less stable temperature profiles are associated with higher relative humidities at upper levels, and vice versa. Thus, even though the interpretation of the constant dsp profiles in terms of relative humidity is not straightforward, the prescription of constant dsp's in the original formulation seems to be too crude. In addition, if the assumption that the shallow convection is a thermodynamically driven process is still to be valid, a reference profile defined in this way should be considered preliminary until the point passes the entropy change test.

The basic idea was that the requirement for the positive entropy change should be incorporated into the specification of the humidity profile rather than constructing a "trial" profile and then testing it for the entropy change. Thus, if

$$\Delta S_T = \sum \left[\frac{c_p(T_{\text{ref}} - T^n)}{T} \right] \Delta p, \tag{3.10}$$

$$\Delta S_q = \sum \left[\frac{L_{\text{wv}}(q_{\text{ref}} - q^n)}{T} \right] \Delta p, \tag{3.11}$$

$$T = \frac{T_{\text{ref}} + T^n}{2}, \tag{3.12}$$

it is required that

$$\Delta S_T + \Delta S_q = \delta, \tag{3.13}$$

where δ is a nonnegative number still to be determined.

The equilibrium moisture profile is defined as a linear function of a suitably chosen function of pressure $Q(p)$; that is,

$$q_{\text{ref}} = q_{\text{reftop}} + c[Q(p) - Q(p_{\text{top}})], \tag{3.14}$$

where

$$c = \frac{\partial q_{\text{ref}}}{\partial Q(p)} = \text{const}, \tag{3.15}$$

and the subscript reftop denotes the value on the reference profile at the cloud top. The two unknown constants in (3.14), q_{reftop} and c, can be determined from (3.13) and the requirement

$$\sum q_{\text{ref}} \Delta p = \sum q^n \Delta p, \tag{3.16}$$

following from the enthalpy conservation constraint (Betts 1986). Namely, taking into account the definitions (3.11) and (3.12), the entropy change formula (3.13) can be rewritten in the form

$$\sum \left[\frac{2L_{wv}(q_{ref} - q^n)}{T_{ref} + T^n}\right] \Delta p = -\Delta S_T + \delta.$$

Combining this formula with (3.16) and (3.14), after some algebra, one obtains

$$a_{11}q_{reftop} + a_{12}c = A$$
$$a_{21}q_{reftop} + a_{22}c = B, \qquad (3.17)$$

where

$$a_{11} = \sum \frac{\Delta p}{T_{ref} + T^n};$$

$$a_{12} = \sum [Q(p) - Q(p_{top})] \frac{\Delta p}{T_{ref} + T^n}$$

$$a_{21} = \sum \Delta p; \quad a_{22} = \sum [Q(p) - Q(p_{top})] \Delta p$$

$$A = \frac{-\Delta S_T + \delta}{2L_{wv}} + \sum \frac{q^n \Delta p}{T_{ref} + T^n}; \quad B = \sum q^n \Delta p. \qquad (3.18)$$

From (3.17) and (3.18), the unknown constants q_{reftop} and c are easily calculated. After testing several other possibilities, the function $Q(p) = T_{ref}(p)$ was chosen.

The yet unanswered question is that of the specification of the entropy change δ in (3.13). According to Betts (1986) and Betts and Miller (1986), the shallow convection is a process operating between buoyant low layers and an inversion aloft. The inversion prevents the occurrence of the penetrative convection. The moisture is transported upward and the heat is transported downward. Note that this requires that in (3.13) the contributions of the heat transport (3.10) and the moisture transport (3.11) be of the opposite signs, that is, negative and positive, respectively. Thus, the shallow convection maintains a delicate balance with a low (if any at all) entropy yield δ.

One of the major concerns with the BM shallow convection scheme was to tune it in such a way as to prevent collapsing of the inversions into the saturated surface layers. The revised shallow convection appears to be less on the defensive side in this respect. In the 48-h integrations of the eta model the cloud tops were slowly rising and the inversions were strengthening with time. The effect on the vertical moisture transport could be detected indirectly through the changes of the precipitation intensity and pattern. All these features showed sensitivity to the specification of δ, which thus appears to be a convenient tuning parameter. As one would expect, by reducing δ, the rising and strengthening of the inversions, as well as the precipitation area and intensity, were reduced.

In practice, the positive contribution of ΔS_q defined by (3.11) is required to be $(1 + \mu)$ times the absolute value of the negative contribution of ΔS_T defined by (3.10), where $\mu = 0.05$. Thus, δ is actually related to $|\Delta S_T|$.

Numerical experimentation revealed that even with the revised scheme there are still conditionally unstable regimes other than the BM deep convection that do not fit into the described image of the shallow convection. In such cases the shallow convection is aborted. For example, ΔS_T can be positive. Also, with $Q(p) = T_{ref}(p)$, the scheme obviously does not work in an atmosphere approaching the isothermal one. The negative slope of the reference humidity profile c, the supersaturation (according to the criterion for the onset of the large-scale precipitation), and the too unstable reference virtual potential temperature profiles (as suggested by Betts) are not allowed. In addition, an absolute upper limit for the shallow cloud tops had to be introduced somewhat above the 500-hPa level. It was found that computational instability may develop over elevated terrain if this limit is exceeded.

4. Surface fluxes and PBL

a. Viscous sublayer: General approach

As reported by Mesinger et al. (1990), a viscous sublayer was incorporated into the eta model following Deardorff (1974) and Zilitinkevitch (1970). This formulation was subsequently replaced by a more elaborate and effective one as described herein.

The viscous sublayer is allowed to operate only over water. The reason for this is that over land a soil slab of finite depth is used in order to describe the evolution of the variables at the lower boundary, so that it is not the surface variables that are used to estimate the surface fluxes but rather the mean values representative of the slab.

Following Liu et al. (1979, hereafter referred to as LKB), in the immediate vicinity of a smooth surface [LKB, Eq. (8)],

$$U_0 - U_S = D_1\left[1 - \exp\left(-\frac{zu_*}{D_1\nu}\right)\right]\left(\frac{F_U}{u_*}\right), \qquad (4.1)$$

$$\theta_0 - \theta_S = D_2\left[1 - \exp\left(-\frac{zu_*}{D_2\chi}\right)\right]\left(\frac{F_\theta}{u_*}\right), \qquad (4.2)$$

$$q_0 - q_S = D_3\left[1 - \exp\left(-\frac{zu_*}{D_3\lambda}\right)\right]\left(\frac{F_q}{u_*}\right). \qquad (4.3)$$

Here, the subscript S denotes the surface values; the subscript 0 (for the time being) indicates the values at a height z above the surface where the molecular diffusivities are still dominant; D_1, D_2, and D_3 are parameters to be discussed in more detail later; u_* is the friction velocity; ν, χ, and λ are the molecular diffusivities for momentum, heat, and water vapor, respectively; and F_U, F_θ, and F_q are the turbulent fluxes of momentum, heat, and water vapor above the viscous sublayer.

For a small argument ζ of the exponential functions in (4.1)–(4.3),

$$\frac{z_U u_*}{D_1 \nu} = \frac{z_\theta u_*}{D_2 \chi} = \frac{z_q u_*}{D_3 \lambda} = \zeta, \tag{4.4}$$

$$1 - \exp(-\zeta) \approx \zeta, \tag{4.5}$$

so that, using (4.4) and (4.5), (4.1)–(4.3) can be approximated by

$$U_0 - U_S = \left(\frac{z_U}{\nu}\right) F_U, \tag{4.6}$$

$$\theta_0 - \theta_S = \left(\frac{z_\theta}{\chi}\right) F_\theta, \tag{4.7}$$

$$q_0 - q_S = \left(\frac{z_q}{\lambda}\right) F_q. \tag{4.8}$$

Here, the heights z_U, z_θ, and z_q are defined by (4.4); that is,

$$z_U = \frac{\zeta \nu D_1}{u_*}, \tag{4.9}$$

$$z_\theta = \frac{\zeta \chi D_2}{u_*}, \tag{4.10}$$

$$z_q = \frac{\zeta \lambda D_3}{u_*}. \tag{4.11}$$

At this point the following simplifying modeling assumptions are made.

- There are two distinct layers: (i) a thin viscous sublayer immediately above the surface, where the vertical transports are determined entirely by the molecular diffusion, and (ii) a turbulent layer above it, where the vertical transports are defined entirely by the turbulent fluxes.
- The depths of the viscous sublayers for the respective physical variables are defined by (4.9)–(4.11) for a chosen fixed value of ζ.

Note that with the definitions of the depths of the viscous sublayers (4.9)–(4.11) the values of the relevant physical quantities at the interfaces of the viscous and the turbulent layers are those denoted by the subscript 0 in (4.6)–(4.8).

Using the Mellor–Yamada level 2 discrete momentum and heat exchange coefficients, $K_{M\mathrm{sfc}}$ and $K_{H\mathrm{sfc}}$, respectively [cf. Janjić 1990, Eqs. (4.6)–(4.7)], the turbulent fluxes in the surface layer above the viscous sublayer are represented by

$$F_U = \left(\frac{K_{M\mathrm{sfc}}}{\Delta z_e}\right)(U_{\mathrm{lm}} - U_0), \tag{4.12}$$

$$F_\theta = \left(\frac{K_{H\mathrm{sfc}}}{\Delta z_e}\right)(\theta_{\mathrm{lm}} - \theta_0), \tag{4.13}$$

$$F_q = \left(\frac{K_{H\mathrm{sfc}}}{\Delta z_e}\right)(q_{\mathrm{lm}} - q_0). \tag{4.14}$$

Here, the subscript lm denotes the variables at the lowest model level, Δz_e is either the equivalent height of the lowest model level that takes into account the presence of the "dynamical turbulence layer" at the bottom of the surface layer (Janjić 1990), or simply $z_{\mathrm{lm}} - z_0$ as in a later modification (Mesinger and Lobocki 1991). In the shallow dynamical turbulence layer the ratio of the height z and the Monin–Obukhov length scale (Monin and Obukhov 1954) is small so that the logarithmic profiles are used [cf. Janjić 1990, Eq. (4.8)].

Substituting (4.12)–(4.14) into (4.6)–(4.8), one obtains

$$\left(\frac{\nu}{z_U}\right)(U_0 - U_S) = \left(\frac{K_{M\mathrm{sfc}}}{\Delta z_e}\right)(U_{\mathrm{lm}} - U_0), \tag{4.15}$$

$$\left(\frac{\chi}{z_\theta}\right)(\theta_0 - \theta_S) = \left(\frac{K_{H\mathrm{sfc}}}{\Delta z_e}\right)(\theta_{\mathrm{lm}} - \theta_0), \tag{4.16}$$

$$\left(\frac{\lambda}{z_q}\right)(q_0 - q_S) = \left(\frac{K_{H\mathrm{sfc}}}{\Delta z_e}\right)(q_{\mathrm{lm}} - q_0). \tag{4.17}$$

Note that (4.15)–(4.17) reflect the requirement for the continuity of the finite-difference fluxes across the interfaces between the two layers. Solving (4.15)–(4.17) for the variables with the subscript 0, one obtains

$$U_0 = \frac{U_S + [(K_{M\mathrm{sfc}} z_U)/(\nu \Delta z_e)] U_{\mathrm{lm}}}{1 + (K_{M\mathrm{sfc}} z_U)/(\nu \Delta z_e)}, \tag{4.18}$$

$$\theta_0 = \frac{\theta_S + [(K_{H\mathrm{sfc}} z_\theta)/(\chi \Delta z_e)] \theta_{\mathrm{lm}}}{1 + (K_{H\mathrm{sfc}} z_\theta)/(\chi \Delta z_e)}, \tag{4.19}$$

$$q_0 = \frac{q_S + [(K_{H\mathrm{sfc}} z_q)/(\lambda \Delta z_e)] q_{\mathrm{lm}}}{1 + (K_{H\mathrm{sfc}} z_q)/(\lambda \Delta z_e)}. \tag{4.20}$$

Thus, the required lower boundary conditions for the turbulent layer are expressed as weighted means of the values at the surface and at the lowest model level. Note that (4.18)–(4.20), together with (4.9)–(4.11), represent a closed system provided the parameters D_1, D_2, D_3, and ζ are known.

The eta model surface layer with the viscous sublayer over the oceans is schematically shown in Fig. 2. In the figure, z_{lm} is the height of the lowest model level and z_i stands for the depths of the viscous sublayers for momentum z_U, heat z_θ, and moisture z_q.

The viscous sublayer over the oceans is assumed to operate in three different regimes: (i) smooth and transitional, (ii) rough, and (iii) rough with spray, depending on the roughness Reynolds number

$$\mathrm{Rr} = \frac{z_0 u_*}{\nu}. \tag{4.21}$$

Here,

$$z_0 = \frac{0.11\nu}{u_*} + \frac{0.018\, u_*^2}{g} \tag{4.22}$$

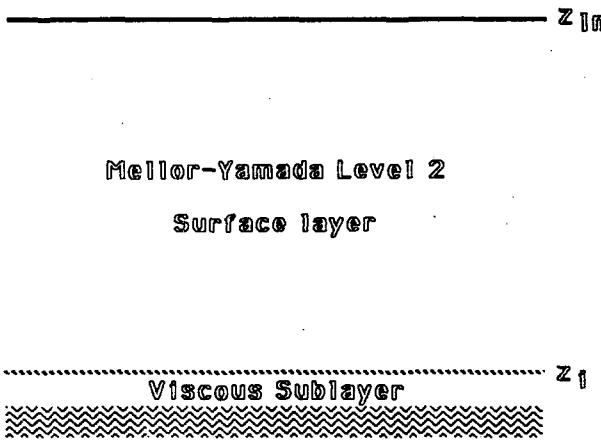

FIG. 2. The eta model surface layer with the viscous sublayer over the oceans. The symbol z_i stands for the depths of the viscous sublayers for momentum, heat, and moisture, and z_{lm} is the height of the lowest model layer.

and

$$u_* = \left[\left(\frac{K_{M\text{sfc}}}{\Delta z_e}\right)(U_{lm} - U_0)\right]^{1/2}. \quad (4.23)$$

Note that the definitions of z_0 and u_* have been changed compared to those of Janjić (1990). The roughness length z_0 as a function of u_* is shown in Fig. 3. When the Reynolds number exceeds a prescribed value Rr_r the flow ceases to be smooth and the rough regime is entered. In the rough regime the momentum is transported also by pressure forces on the roughness elements so that (4.1) loses validity (LKB). Consequently, the viscous sublayer for momentum is turned off. However, for heat and moisture, the viscous sublayer is still operating until the rough regime with spray is reached at a critical value Rr_s when the viscous sublayer collapses completely. In the rough regime with spray the breaking waves and the spray are assumed to provide a much more efficient way of exchange of heat and moisture between the ocean and the air than can be accomplished by the molecular viscosity. Note that instead of in terms of Rr the boundaries between the regimes can be also defined in terms of u_*, since Rr is a monotonic function of u_*.

b. Determination of the parameters

For the parameters D_1, D_2, and D_3 appearing in (4.1)–(4.3), LKB suggest [Eq. (11)]

$$D_1 = M\,\text{Rr}^{1/4} \quad (4.24)$$

$$D_2 = M\,\text{Rr}^{1/4}\,\text{Pr}^{1/2} \quad (4.25)$$

$$D_3 = M\,\text{Rr}^{1/4}\,\text{Sc}^{1/2}, \quad (4.26)$$

where $\text{Pr} = \nu/\chi$ is the Prandtl number, $\text{Sc} = \nu/\lambda$ is the Schmidt number, and M is a constant, but different for different regimes. With these definitions and the definition (4.21), (4.9)–(4.11) take the form

$$z_U = \frac{\zeta\nu}{u_*}\left[M\left(\frac{z_0 u_*}{\nu}\right)^{1/4}\right] \quad (4.27)$$

$$z_T = \frac{\zeta\chi}{u_*}\left[M\left(\frac{z_0 u_*}{\nu}\right)^{1/4}\text{Pr}^{1/2}\right] \quad (4.28)$$

$$z_q = \frac{\zeta\lambda}{u_*}\left[M\left(\frac{z_0 u_*}{\nu}\right)^{1/4}\text{Sc}^{1/2}\right]. \quad (4.29)$$

For the smooth regime LKB used the value of M, which was close to 30. When the flow ceases to be smooth they suggest the value of about 10, which fits best the Mangarella et al. (1973) data. These two values are also applied in the eta model for the corresponding regimes. At the present level of approximation, the Prandtl number and the Schmidt number were as-

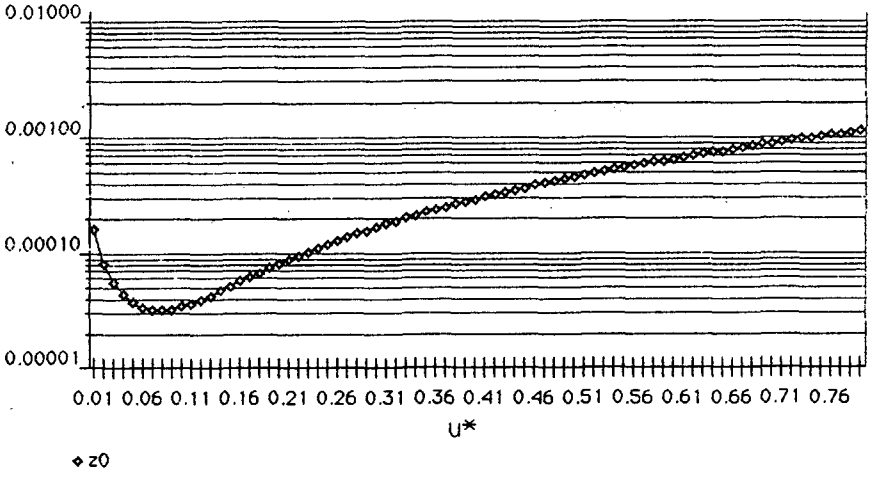

FIG. 3. The roughness length z_0 (m) as a function of u_* (m s^{-1}).

sumed to be the same—that is, Pr = Sc = 0.71—and the molecular viscosity for momentum was $\nu = 0.000015$. The molecular diffusion coefficients for heat and moisture, χ and λ, are determined by ν, Pr, and Sc.

Concerning the values of the Reynolds number at which the transitions between the different regimes occur, they are determined empirically. Subjectively judged, the best results in the two cases considered were obtained with $\mathrm{Rr}_r = 3.4$ and $\mathrm{Rr}_s = 42$, or in terms of u_*, with the values $u_{*r} = 0.30$ m s^{-1} and $u_{*s} = 0.70$ m s^{-1}, respectively. These values qualitatively agree in the order of magnitude with the laboratory measurements (2–3 for Rr_r and 50–80 for Rr_s). A better agreement is probably hard to expect.

With $\zeta = 0.50$, and the chosen values of the other parameters, the depths (4.27)–(4.29) in meters are shown in Fig. 4 as functions of u_* for various turbulent regimes. Note the changes of the regimes at $u_{*r} = 0.30$ m s^{-1} and $u_{*s} = 0.70$ m s^{-1}.

In the practical implementation, u_* for the current time step is calculated from (4.23) using $K_{M\mathrm{sfc}}$ and U_0 from the previous time step. Thus obtained, u_* is then used in (4.22) to update z_0. With the depths z_U, z_T, and z_q being calculated from (4.27)–(4.29), the lower boundary conditions for the Mellor–Yamada level 2 surface layer U_0, θ_0, and q_0 can now be obtained from (4.18)–(4.20) using $K_{M\mathrm{sfc}}$ and $K_{H\mathrm{sfc}}$ from the previous time step. However, in order to prevent the two-grid-interval oscillation in time, the average values of U_0, θ_0, and q_0 from the present and the previous time steps are actually used.

c. *Mellor–Yamada level 2.5*

As a deviation from the usual practice, in the eta model TKE is initialized from above within the PBL in order to preserve the ability of the level 2.5 scheme to respond quickly to possible large thermal instabilities in the initial conditions and to speed up the PBL spinup. In this way the level 2.5 scheme is dissipating excessive TKE rather than producing it at most places during the PBL spinup period.

An aspect of the level 2.5 scheme that was also reexamined in some detail is the definition of the master length scale l. As already pointed out, several methods have been proposed for estimating this quantity (e.g., Zilitinkevitch 1970; Mellor and Yamada 1974, 1982; Galperin et al. 1988). In the eta model the diagnostic formula [Mellor and Yamada 1974; Miyakoda and Sirutis 1977; Janjić 1990, Eqs. (3.8)] of the form

$$l = \frac{l_0 \kappa z}{\kappa z + l_0}, \quad l_0 = \alpha \frac{\int_{p_T}^{p_S} |z| q\, dp}{\int_{p_T}^{p_s} q\, dp}, \quad \alpha = \text{const} \tag{4.30}$$

was used for some time. In (4.30), p_S and p_T are pressures at the bottom and at the top of the model atmosphere, respectively, κ is the von Kármán constant, and α is an empirical constant. Note that in the Blackadar formula [the first one in (4.30)] l tends to κz for small z and to an asymptotic value l_0 when z becomes large. An upper limit was imposed on l_0, and following Galperin et al. (1988), in stably stratified flows l was not allowed to exceed

$$0.53q\left(\beta g \frac{\partial \Theta}{\partial z}\right)^{-1/2} + H, \tag{4.31}$$

where H was a positive constant. The Galperin et al. (1988) formula alone [i.e., the formula (4.31) with $H = 0$] was producing too small values of l in unstable

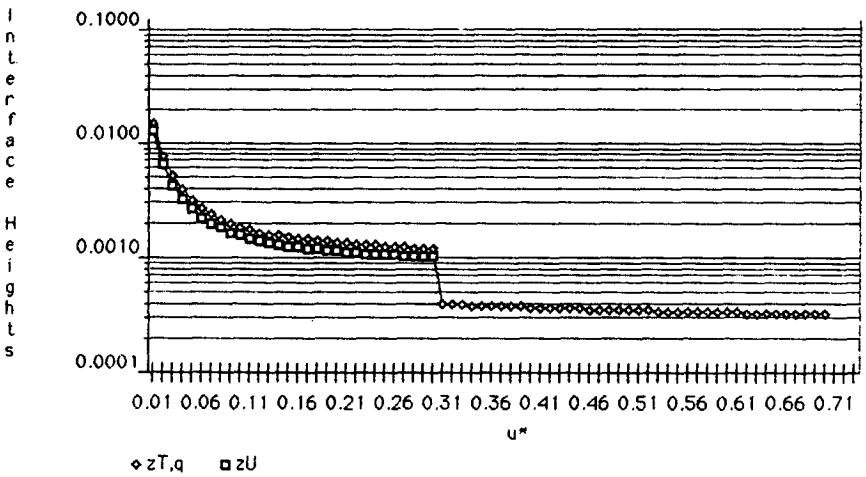

FIG. 4. The depths z_U, z_T, and z_q (m) as functions of u_* (m s^{-1}) in various turbulent regimes. Note the jumps at $u_* = 0.30$ and 0.70 m s^{-1}.

regimes. In addition to this technique, the methods tested in the eta model included those of Zilitinkevitch (1970), as well as Blackadar style formulas combined with prescribed constant l_0, or l proportional to the vertical resolution at upper levels. A systematic overall impact of the changes could not be identified as long as the values of l in the PBL were of the order of those obtained by Mellor and Yamada (1974) and Janjić (1990). The exception was very large l's within the PBL, which tended to make the precipitation problem worse. Thus, sufficient justification for abandoning or modifying the method (4.30) could not be found, particularly in view of the rectification of the procedure for the computation of l_0 described in the next subsection.

d. *Mellor–Yamada level 2 and the surface fluxes*

Reexamining the performance of the surface layer, (as suspected by Betts) it was found that in near-neutral conditions with weak wind over water, the equivalent bulk aerodynamic coefficients estimated from the level 2 fluxes could be several times larger than those measured under similar conditions. The only major difference was that the water temperature was 4°C in the measurements and over 25°C in the experiments.

As can be seen from Mellor and Yamada (1982) or Janjić [1990, Eqs. (4.6) and (4.7)], for example, the turbulent exchange coefficients for momentum $K_{M\text{sfc}}$ and heat $K_{H\text{sfc}}$ are proportional to the square of the length scale l. The length scale l was assumed to vary linearly with z reaching the value of the level 2.5 master length scale (4.30) and (4.31) at the top of the lowest model layer (Janjić 1990).

The most straightforward response to the problem would be to impose an ad hoc low upper limit on l. However, as discussed previously, this was considered to be a dangerous practice that could inhibit the ability of the model to produce large surface fluxes needed to feed tropical storms, for example. Fortunately, any action of this kind turned out to be unnecessary. The problem was found to be due to an inconsistency in the implementation of the method (4.30) and (4.31). When calculating the integrals in the formula for l_0, all values of q were used, including those at the points where q^2 was set to its minimum allowed value. This lower limit acts as zero for q^2 and should not have been taken into account. For example, if there is no TKE in the entire column, that is, if q^2 is set to its minimum value, the formula for l_0 in (4.30) would nevertheless yield the maximum value. When this inconsistency was removed, the level 2.5 l's were reduced, and the restriction (4.31) was lifted as it became unnecessary.

With the near-neutral stratification of the marine surface layer and the weak wind, a deep PBL does not develop, so that after eliminating the inconsistency, the level 2.5 l's obtained from formula (4.30) remained well below their prescribed maximum allowed values. Being calculated from the level 2.5 master length scale, the level 2 l's in the surface layer were considerably reduced as well, so that the computed marine surface fluxes dropped to, or below, the measured values. However, in order to be on the safe side, the parameter α appearing in (4.30) was reduced to 0.075 over the sea. The problems with the surface layer and the PBL over land were different, so that α was increased to 0.20 in order to avoid the reduction of the level 2.5 master length scale and consequently the level 2 l's in the surface layer. More specifically, during the cold part of the year some cyclones with stable or near-neutral surface layers tended to overdevelop due to insufficient surface friction. In such a situation, the reduction of the level 2 l's could only aggravate the problem. To avoid large underestimation of the level 2 fluxes in the near-neutral conditions, particularly in the marine surface layer, a lower limit was prescribed for the level 2 l's.

The described modifications had little effect on the forecasts. This is not surprising considering that there has been little difficulty with the near-neutral marine surface layers with weak wind. The problems have always been associated with strong thermal instabilities.

5. Review of major experimental results

The sensitivity to the reformulated shallow convection and the rectification and retuning of the PBL schemes were discussed in more detail in the corresponding subsections. One may recall that the revised shallow convection had a detectable impact on the forecasts, while it was much less so with the PBL changes.

To demonstrate the effects of the reformulated BM scheme for the deep convection and the newly designed viscous sublayer scheme, two summer cases were used. Recall that in the case starting at 0000 UTC 20 July 1989, an unsuccessful 48-h forecast with heavy spurious precipitation over warm water was obtained. As demonstrated by Black et al. (1989), in contrast to that in the case of 0000 UTC 31 July 1989, the version of the model run quasi-operationally at NMC produced a successful 36-h forecast of the development of the Tropical Storm Chantal. In the control runs, the BM deep convection scheme without the modifications was applied and the viscous sublayer was turned off.

In Fig. 5, the verifying mean sea level pressure analysis valid at 0000 UTC 22 July 1989 is shown (left panel), together with the verifying analysis of the accumulated 24-h précipitation valid at 1200 UTC 21 July 1989 (right panel). Note that the precipitation verifications are available only at 1200 UTC, and at the time of the study were produced only over the eastern part of the United States. The verification data shown are defined on a grid with the resolution of about 190 km. Nevertheless, the verification map can be used at least for a qualitative assessment of the 36-h precipitation forecasts.

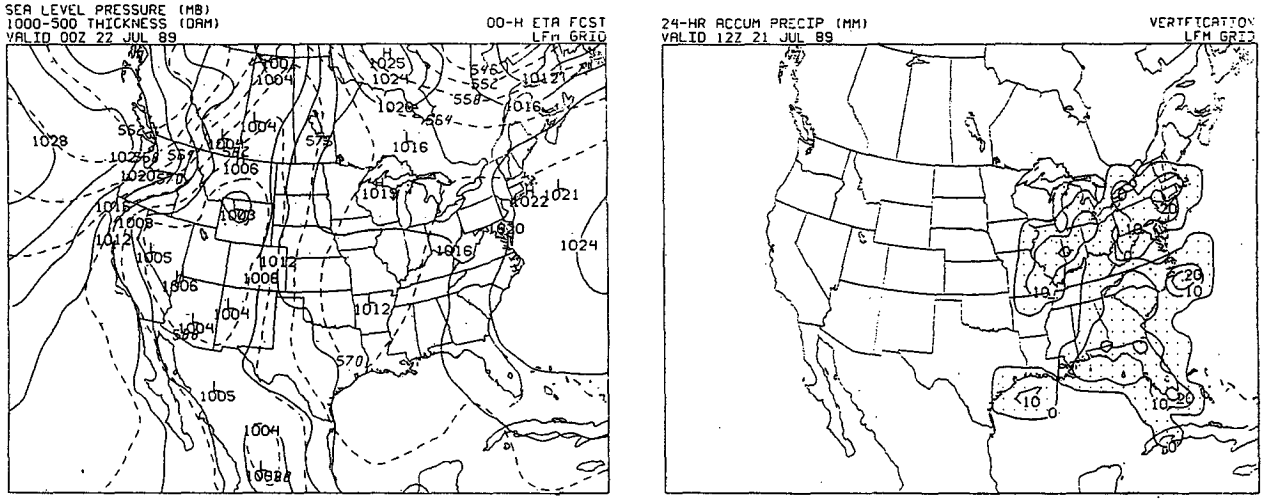

FIG. 5. Verifying mean sea level pressure analysis valid at 0000 UTC 22 July 1989 (left panel), and verifying accumulated 24-h precipitation analysis valid at 1200 UTC 21 July 1989 (right panel).

The forecasts of the mean sea level pressure valid at 0000 UTC 22 July 1989 obtained in the 48-h test runs are presented in Fig. 6. The control forecast with the BM deep convection scheme and without the viscous sublayer (upper left panel), the forecast with the revised deep convection but without the viscous sublayer (upper right panel), the forecast with the BM deep convection scheme but with the new viscous sublayer scheme (lower left panel), and the forecast with the revised deep convection and the new viscous sublayer scheme (lower right panel) are displayed. As can be seen from the figure, in the control run (upper left panel) a spurious cyclone with two closed isobars and the central mean sea level pressure of 997 hPa developed over the northeastern part of the Gulf of Mexico and adjacent southern states. The center of the cyclone was at the coastline of the western part of Florida. The observed pressure at this location was about 1017 hPa. When applied separately, the revised deep convection scheme (upper right panel) and the newly designed viscous sublayer scheme (lower left panel) each correctly shifted the center of the low westward, but the revised BM scheme more so than the viscous sublayer. The revised convection scheme (upper right panel) was also more successful in increasing the pressure in the center of the coastal low to 1007 hPa, as compared to 1006 hPa in the case of the new viscous sublayer (lower left panel). The pressures at the location of the center of the coastal cyclone in the control run were increased by the two schemes by about 12 and 11 hPa, respectively. Both schemes developed secondary lows farther north over land: over Alabama in the case of the revised BM scheme, and farther west over Mississippi in the case of the viscous sublayer. With the two new schemes applied in combination (lower right panel), the coastal cyclone and the northern low over land filled further and merged into an elongated weak trough extending in the north–south direction. The pressure at the location of the center of the coastal cyclone in the control run increased by about 17 hPa to about 1014 hPa. Thus, with the two new schemes applied in combination, a good 48-h mean sea level pressure forecast was obtained, which in the critical areas agreed within about 2 hPa with the verifying analysis shown in the left panel of Fig. 5.

The 36-h test forecasts of the accumulated 24-h precipitation valid at 1200 UTC 21 July 1989 are presented in Fig. 7. The control forecast (left panel) and the forecast with the revised deep convection and the new viscous sublayer scheme (right panel) are shown. In the control run, vast areas of sustained heavy precipitation developed over the sea by the second day of the forecast. The precipitation maximum off the coast of western Florida exceeded 210 mm. This heavy precipitation area extended to the southeast reaching the secondary maximum of over 90 mm northwest off the western tip of Cuba. The third, smaller and more isolated maximum of over 50 mm was located off the coast of the Carolinas. Light (and at places not so light) precipitation covered most of the west Atlantic and was also spread over vast areas of the east Pacific. The described precipitation forecast over sea could not be verified due to the lack of the observed data. However, as can be seen from the verification map in the right panel of Fig. 5, at least in the southern and eastern coastal areas, as well as over western Cuba, the precipitation was generally largely overpredicted. At the same time, the observed offshore precipitation maximum south of the Texas–Louisiana border did not appear in the forecast. Farther inland, the precipitation was heavier than in the verification map over parts of Alabama and Georgia, and too light in the Carolinas. The precipitation was also too light in the tongue protruding from the northeast into Arkansas. In addition,

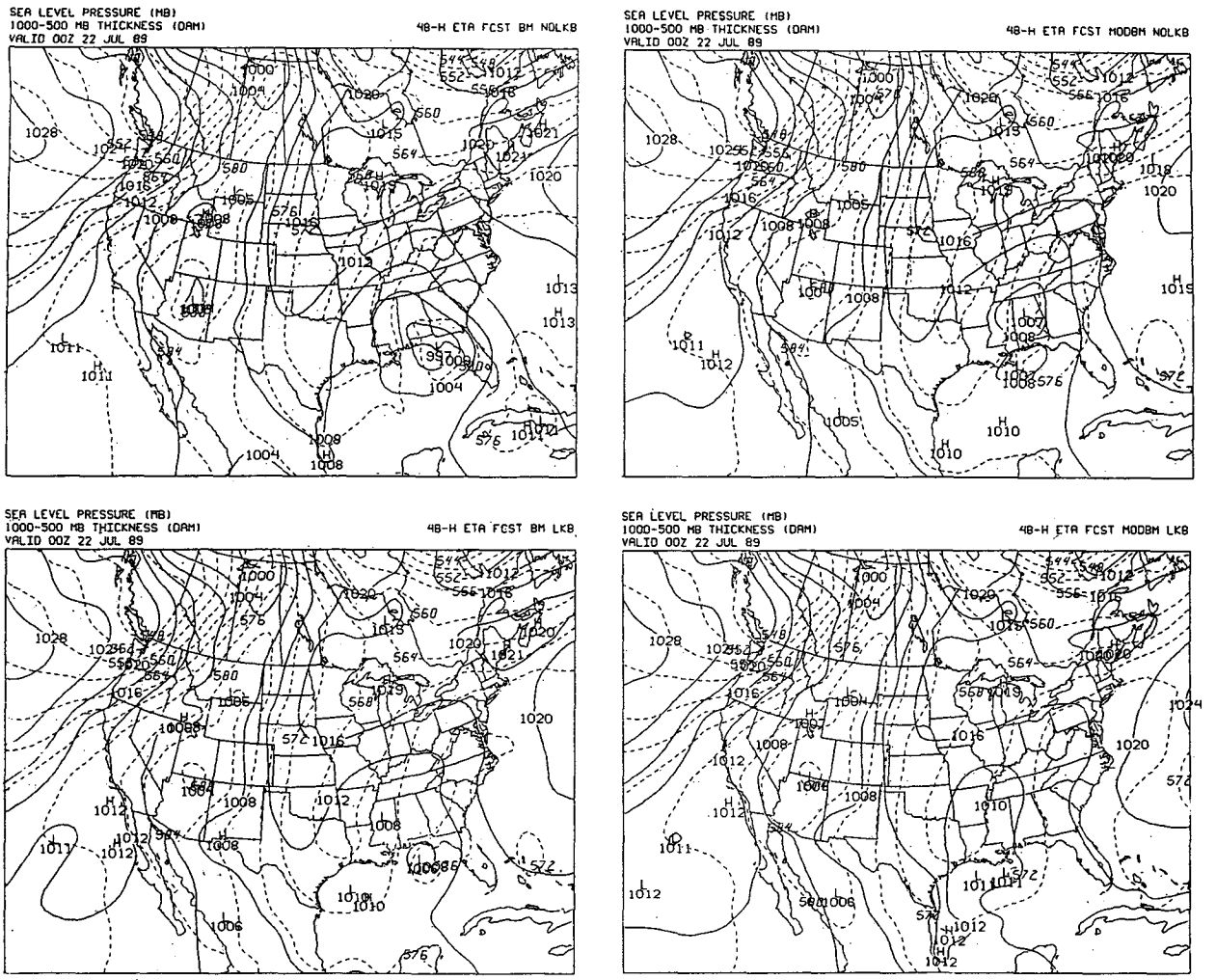

FIG. 6. Forecasts of mean sea level pressure valid at 0000 UTC 22 July 1989 obtained in 48-h test runs starting from 0000 UTC 20 July 1989. The control forecast with the BM deep convection scheme and without the viscous sublayer (upper left panel), the forecast with the revised deep convection but without the viscous sublayer (upper right panel), the forecast with the BM deep convection scheme but with the new viscous sublayer scheme (lower left panel), and the forecast with the revised deep convection and the new viscous sublayer scheme (lower right panel) are displayed.

the light precipitation over land did not cover a sufficiently large area.

As can be seen from the right panel of Fig. 7, with the revised deep convection and the new viscous sublayer scheme, the areas of heavy precipitation over the sea disappeared. The heavy precipitation area appearing in the control run in the Gulf of Mexico was greatly reduced. The precipitation maximum moved north across the coastline of western Florida and decreased to just over 40 mm. The secondary heavy precipitation area extending to the southeast in the Caribbean Sea vanished. Only a disconnected area of light precipitation was left over the western part of Cuba and adjacent waters. The smaller and more isolated maximum off the coast of the Carolinas moved slightly northeast, toward Cape Hatteras, and its intensity was reduced to just over 20 mm. Considerable areas of light precipitation over the oceans were mopped up, particularly in the east Pacific. As can be seen from the verification map in the right panel of Fig. 5, the precipitation forecast in the southern and eastern coastal areas, as well as over Cuba, was generally greatly improved. The amount of the predicted accumulated precipitation in these areas agrees qualitatively with the observed values, although the observed offshore maximum south of the Texas–Louisiana border is still missing. The predicted value and the location of the maximum off the coast of Carolinas were also improved. Farther inland, the precipitation was still heavier than in the verification map over parts of Florida, Alabama, and Georgia, and too light in the Carolinas. A qualitative improvement was achieved by producing more precipitation inside the tongue protruding from the northeast into Arkansas. However, the location of the newly devel-

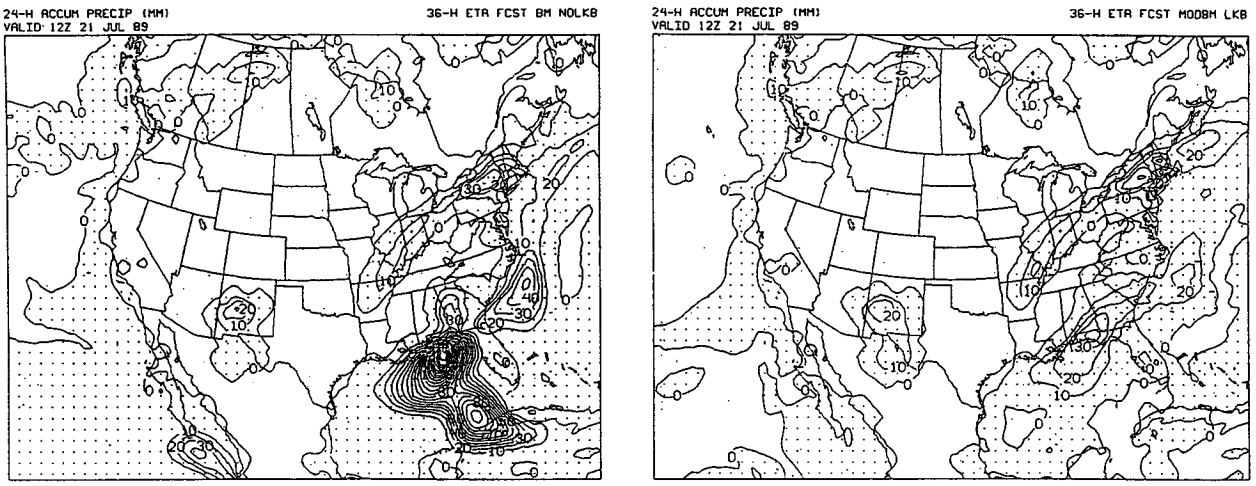

FIG. 7. Forecasts of the accumulated 24-h precipitation valid at 1200 UTC 21 July 1989 obtained in 36-h test runs starting from 0000 UTC 20 July 1989. The control forecast with the BM deep convection scheme and without the viscous sublayer (left panel) and the forecast with the revised deep convection and the new viscous sublayer scheme (right panel) are displayed.

oped maximum exceeding 20 mm did not coincide with that of the maximum in the verification map. Finally, as another step in the right direction, the area of the light precipitation over land was visibly larger than in the control run.

In the case considered, the occurrence of the well-developed spurious low over warm water was accompanied by the unrealistically heavy precipitation. This has been no exception. As a rule, the development of spurious lows over warm water coincides with heavy precipitation.

With the heavy spurious precipitation of the 0000 UTC 20 July 1989 case under control, the question arises as to whether the modifications introduced impair the ability of the model to forecast the heavy precipitation events such as tropical storms. To find out, the model was run starting from the 0000 UTC 31 July 1989 data.

At 1200 UTC 1 August 1989, the center of the Tropical Storm Chantal was off the coast of Texas, south of the Texas–Louisiana border (cf. Black et al. 1989; Climate Analysis Center 1989). Over the next 12 h, the storm advanced northwest across the coast of Texas, filling quickly. By 0000 UTC 2 August 1989, the center of the storm was far inland, and the tropical cyclone turned into a weak low in the mean sea level pressure with the closed 1008-hPa isobar (cf. Climate Analysis Center 1989).

The 36- and 48-h forecasts of the mean sea level pressure obtained in the test runs starting from 0000 UTC 31 July 1989 are presented in Fig. 8. The 36-h control forecast with the BM deep convection scheme and without the viscous sublayer (upper left panel), the 36-h forecast with the revised deep convection and the new viscous sublayer scheme (upper right panel), the 48-h control forecast with the BM deep convection scheme and without the viscous sublayer (lower left panel), and the 48-h forecast with the revised deep convection and the new viscous sublayer scheme (lower right panel) are displayed. In the 36-h control forecast (upper left panel) verifying at 1200 UTC 1 August 1989 the cyclone was well developed. There were five closed isobars, and the pressure at the cyclone center was about right (cf. Black et al. 1989). However, the size of the vortex was overestimated. The center of the cyclone was over the sea, somewhat on the Louisiana side south of the Texas–Louisiana border. Over the next 12 h of the control forecast, the cyclone was moving over water predominantly westward. It was filling but not quickly enough. In the 48-h forecast (lower left panel) verifying at 0000 UTC 2 August 1989, the cyclone finally reached the coast of Texas. However, the center of the cyclone stayed over water.

In the 36-h forecast with the revised deep convection and the new viscous sublayer scheme (upper right panel) verifying at 1200 UTC 1 August 1989, the cyclone was also well developed but somewhat less than before. There were four closed isobars and the pressure at the cyclone center was slightly overpredicted (cf. Black et al. 1989). Note that one can hardly expect the correct forecast of the central pressure with the horizontal resolution of 80 km. The size of the vortex was somewhat reduced compared to the control run. The center of the cyclone was still over the sea south of the Texas–Louisiana border. However, careful inspection reveals a slight improvement of the predicted track. Over the next 12 h of the forecast, the improvement of the track becomes evident. The storm advanced north-northwest across the coast of Texas, filling, but not quickly enough. In the 48-h forecast (lower right panel) verifying at 0000 UTC 2 August 1989 the center of the storm was far inland. However, the cy-

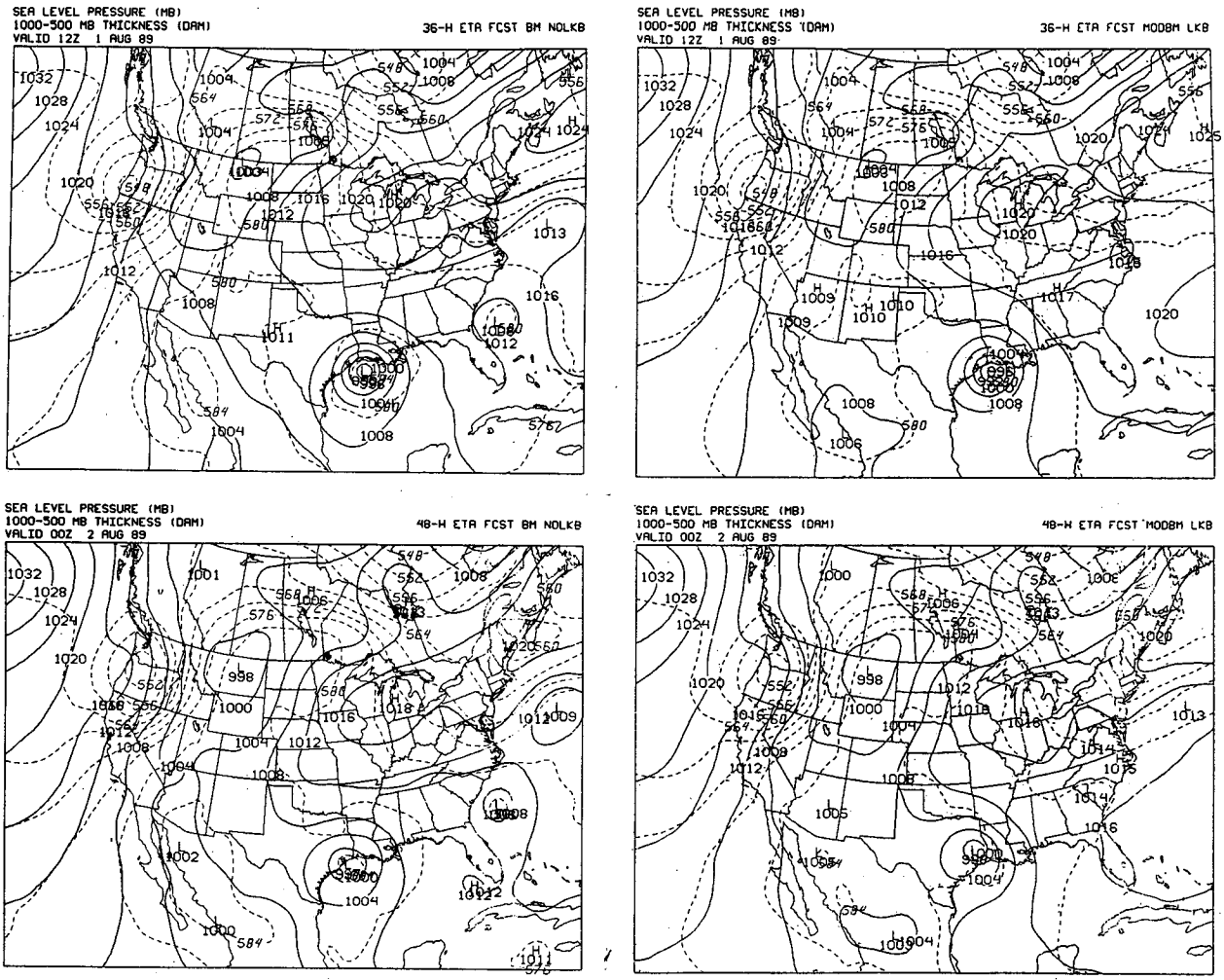

FIG. 8. Forecasts of mean sea level pressure obtained in 36- and 48-h test runs starting from 0000 UTC 31 July 1989. The 36-h control forecast with the BM deep convection scheme and without the viscous sublayer (upper left panel), the 36-h forecast with the revised deep convection and the new viscous sublayer scheme (upper right panel), the 48-h control forecast with the BM deep convection scheme and without the viscous sublayer (lower left panel), and the 48-h forecast with the revised deep convection and the new viscous sublayer scheme (lower right panel) are displayed.

clone stayed east-southeast of the observed location, and the pressure at its center remained too low (cf. Climate Analysis Center 1989).

6. Conclusions and review of further efforts

The eta model has demonstrated a remarkable skill in forecasting the development and movement of severe storms (Black and Mesinger 1989, 1991; Black et al. 1989, 1990; Lazić 1990, 1993a,b; Lazić and Telenta 1990; Mesinger and Black 1989, 1991; Mesinger et al. 1990; Rogers et al. 1991; Ward 1990; WGNE 1989, 1990). However, it was also occasionally producing heavy spurious precipitation over warm water, as well as widely spread light precipitation over oceans. In addition, the convective forcing, particularly the shallow one, could produce negative entropy changes.

Looking for the possible causes of the problems, three major areas of research were identified: (i) the deep and the shallow convection schemes, (ii) the processes at the interface between the sea and the air, and (iii) the Mellor–Yamada level 2 and level 2.5 schemes. As the outcome, (i) a major revision of the BM scheme over the oceans was made, (ii) a new flexible viscous sublayer scheme was designed, and (iii) the Mellor–Yamada level 2 and level 2.5 schemes were retuned.

The deep convective regimes are postulated to be characterized by a parameter called "cloud efficiency." The relaxation time is extended for low cloud efficiencies, and vice versa. It is also postulated that there is a range of reference equilibrium states instead of a single one. The specific reference state is chosen depending on the cloud efficiency. The treatment of the shallow cloud tops was modified, and the shallow reference hu-

midity profiles are specified requiring that the entropy change be nonnegative.

Two layers are introduced over the oceans: (a) a viscous sublayer with the vertical transports determined entirely by the molecular diffusion, and (b) a layer above it with the vertical transports determined only by the turbulence. The viscous sublayer operates in different regimes depending on the roughness Reynolds number.

The MY level 2.5 TKE is initialized "from above" in the PBL, so that excessive TKE is dissipated at most places during the PBL spinup. The method used for calculating the MY level 2.5 master length scale was rectified. In this way, possible overestimation of the level 2 surface fluxes over water is also avoided in the case of near-neutral conditions with weak wind.

To demonstrate the effects of the new schemes for the deep convection and the viscous sublayer, tests were made using two summer cases: one with heavy spurious precipitation, and another when the version of the model run quasi-operationally at NMC Washington produced a successful 36-h forecast of a tropical cyclone (Black et al. 1989). In the case with the excessive precipitation, each of the two schemes had large and about equal positive impacts on the mean sea level pressure forecasts. In contrast to the control run, the new schemes used in combination resulted in a successful 48-h forecast of the mean sea level pressure. The 36-h predicted accumulated 24-h precipitation was brought much closer to reality. The results were also favorable in the tropical storm case in the sense that the ability of the model to predict its development was preserved. In addition, compared to the control run, the cyclone track was noticeably improved, particularly at the later stages of the forecast.

Early attempts to apply the unified convection scheme over both sea and land resulted in a slight degradation of the precipitation scores over land. However, experiments performed at NMC demonstrated that the precipitation scores can be noticeably improved, extending the new concept over land but using dryer humidity profiles (F. Mesinger 1991, personal communication).

Despite the successes of the newly designed convection and viscous sublayer schemes, the episodes of excessive precipitation and overdevelopments of the associated systems over warm water have not been completely eliminated. These episodes often have been associated with pathological features in the initial conditions such as strong instability in terms of the virtual potential temperature in the surface layer accompanied by strong wind at the lowest eta model level. Such features can hardly be found in nature and are suspected to be a result of inconsistencies between the eta model and the assimilation system.

Naturally, atmospheric models are continuously evolving and, therefore, it is not advisable to discuss too specific details of a model, particularly the tuning constants. This principle was not strictly followed here in order to make the experimental results reproducible. The specifics presented in the paper were incorporated into the eta model in 1990 and do not necessarily coincide with those of the latest version of the model, which has become operational at NMC in June 1993. It is hoped that more details on further developments will be reported elsewhere. For example, subsequent to the research reported here, some details of the deep convection algorithm have been modified at NMC (J. P. Gerrity 1992, personal communication). Also, the problem of the surface fluxes was readdressed by Mesinger and Lobocki (1991). Another modification relevant for the surface fluxes calculations was adding a thin lowest eta layer (F. Mesinger, personal communication). Although the increased resolution is always welcome, such a layer represents a deviation from the basic eta coordinate philosophy that requires high vertical resolution and approximately equidistant eta surfaces in the lower troposphere in order to resolve the mountains well and to treat the interactions between the atmosphere and the underlying surface approximately equally both over low-lying and elevated terrain. For this reason, relatively deep surface layers have been used in most experiments with the eta model, so that the surface layer has remained a potentially weak point and thus an area naturally attracting scientific interest.

Acknowledgments. This research was supported by the University Corporation for Atmospheric Research (UCAR). The work reported here was done during the author's visit to NMC, Washington, D.C., in 1989 and 1990. The experimental results presented, and most of those referred to, were produced using the NMC databases and computer facilities. The author is indebted to Dr. Thomas L. Black of NMC for many useful discussions, as well as for handling the interfaces with the NMC data archives, graphics and data reformatting, reinterpolations, and conversions. On several occasions, his suggestions on the model parameters to be looked at facilitated early identification and elimination of several problems. While working on the convection scheme, the author had the privilege of several long and productive discussions with Dr. Alan Betts, who is given credit for his contributions in the text of the paper. The author is also indebted to Mr. B. Telenta of the Federal Hydrometeorological Institute, who brought to the author's attention the entropy changes observed in Mr. Telenta's 3D convective cloud model. The meticulous work of Dr. Joe Gerrity of NMC on the diagnostics and performance of the convection schemes prompted and influenced the direction of the research reported. The support of Dr. Eugenia Kalnay that the author enjoyed was certainly most helpful. The author is indebted to Ms. Dušanka Županski for rerunning the test cases discussed in the paper and for producing the plots. Many contacts with Prof. Fedor

Mesinger helped to finalize the text of the paper. The author also wishes to thank numerous other people he contacted during the visit and had productive discussions with and to whom injustice is done by not mentioning them by name. In the early planning and decision-making period and in the preparation of the paper the author had the support of the Association for Science of Serbia. In addition, the author is grateful for the most efficient and effective handling of a number of practical problems by Ms. Meg Austin, Dr. Bill Curtis, and all other nice UCAR people. Finally, the author wishes to thank to his family for support, and his nurse, Ms. Jadranka Zdravković.

REFERENCES

Betts, A. K., 1986: A new convective adjustment scheme. Part I: Observational and theoretical basis. *Quart. J. Roy. Meteor. Soc.*, **112,** 677–691.

——, and M. J. Miller, 1986: A new convective adjustment scheme. Part II: Single column tests using GATE wave, BOMEX and arctic air-mass data sets. *Quart. J. Roy. Meteor. Soc.*, **112,** 693–709.

Black, T. L., 1988: The step-mountain, eta coordinate regional model: A documentation. NOAA/NWS/NMC, 47 pp. [Available from the Development Division, W/NMC2, WWB, Room 204, Washington, D.C. 20233.]

——, and Z. I. Janjić, 1988: Preliminary forecast results from a step-mountain eta coordinate regional model. *Eighth Conf. on Numerical Weather Prediction,* Baltimore, Amer. Meteor. Soc., 442–447.

——, and F. Mesinger, 1989: Forecast performance of NMC's eta coordinate regional model. *12th Conf. on Weather Analysis and Forecasting,* Monterey, CA, Amer. Meteor. Soc., 551–555.

——, and ——, 1991: Small scale circulations in NMC's 30 km eta model. *Ninth Conf. on Numerical Weather Prediction,* Denver, CO, Amer. Meteor. Soc., 213–216.

——, J. H. Ward, and Z. I. Janjić, 1989: Tropical storm forecasts using Betts–Miller convection in NMC's eta coordinate regional model. Research Activities in Atmospheric and Oceanic Modelling, WCRP, No. 13, 5.38–5.39.

——, Z. I. Janjić, and J. H. Ward, 1990: Heavy precipitation forecasts from NMC's eta model. *16th Conf. on Severe Local Storms,* Kananaskis Park, Alberta, Canada, Amer. Meteor. Soc., J1–J4.

Carpenter, R. L., Jr., K. K. Droegemeier, P. W. Woodward, and C. E. Hane, 1990: Application of the piecewise parabolic method (PPM) to meteorological modeling. *Mon. Wea. Rev.*, **118,** 586–612.

Climate Analysis Center, 1989: Daily Weather Maps. Weekly Series, 31 July–6 August 1989. [Available from the Climate Analysis Center, Room 808, 5200 Auth Road, Camp Springs, MD 20746.]

Davies, R., 1982: Documentation of the solar radiation parametrization in the GLAS climate model. NASA Tech. Memo. 83961, 57 pp. [Available from the Goddard Space Flight Center, Greenbelt, MD 20771.]

Deardorff, J. W., 1974: Three-dimensional numerical study of the height and mean structure of a heated planetary boundary layer. *Bound.-Layer Meteor.*, **7,** 81–106.

Galperin, B., L. H. Kantha, S. Hassid, and A. Rosati, 1988: A quasi-equilibrium turbulent energy model for geophysical flows. *J. Atmos. Sci.*, **45,** 55–62.

Gerrity, J. P., and T. L. Black, 1987: Exposition of the HIBU model formulation of the turbulent transfer process. NOAA/NWS/NMC, 14 pp. [Available from the Development Division, W/NMC2, WWB, Room 204, Washington, D.C. 20233.]

Harshvardhan, and D. G. Corsetti, 1984: Longwave radiation parametrization for the UCLA/GLAS GCM. NASA Tech. Memo. 86072, 48 pp. [Available from the Goddard Space Flight Center, Greenbelt, MD 20771.]

Janjić, Z. I., 1974: A stable centered difference scheme free of two-grid-interval noise. *Mon. Wea. Rev.*, **102,** 319–323.

——, 1979: Forward–backward scheme modified to prevent two-grid-interval noise and its application in sigma coordinate models. *Contrib. Atmos. Phys.*, **52,** 69–84.

——, 1984a: Non-linear advection schemes and energy cascade on semi-staggered grids. *Mon. Wea. Rev.*, **112,** 1234–1245.

——, 1984b: Non-linear advection Eulerian schemes. Workshop on limited area numerical weather prediction models for computers of limited power. Part I. Programme on short- and medium-range weather prediction research, PSMP Report Series No. 8, WMO, 117–156. [Available from the Case Postale 2300, CH-1211 Geneve 2.]

——, 1988a: Regional numerical weather prediction: Problems and some examples. *12th IMACS World Congress '88 on Scientific Computation,* Paris, Intern. Associat. for Mathem. and Computers in Simulation.

——, 1988b: Numerical Techniques for the Physics in NWP. WMO technical conference on regional weather prediction with emphasis on the use of global products, programme on short- and medium-range weather prediction research, PSMP Report Series No. 27, WMO, 191–193. [Available from Case Postale 2300, CH-1211 Geneve 2.]

——, 1990: The step-mountain coordinate: Physical package. *Mon. Wea. Rev.*, **118,** 1429–1443.

——, and F. Mesinger, 1984: Finite difference methods for the shallow water equations on various horizontal grids. *Numerical Methods for Weather Prediction, Seminar 1983,* Reading, United Kingdom, ECMWF, 29–101. [Available from ECMWF, Shinfield Park, Reading, Berkshire RG2 9AX, U.K.]

——, and L. Lazić, 1988: Feasibility study on the application of the HIBU model with included physical package (excluding radiation) into the operational practice of FHMI. Tech. Rep., Department of Meteorology, University of Belgrade, 20 pp (in Serbian).

——, F. Mesinger, and T. L. Black, 1988a: Horizontal discretization and forcing. *Techniques for Horizontal Discretization in Numerical Weather Prediction Models, Workshop,* Reading, United Kingdom, ECMWF, 207–227.

——, T. L. Black, L. Lazić, and F. Mesinger, 1988b: Forecast sensitivity to the choice of the vertical coordinate. *Ann. Geophys.* 147.

Lazić, L., 1990: Forecasts of AMEX tropical cyclones with step-mountain model. *Aust. Meteor. Mag.*, **38,** 207–216.

——, 1993a: Eta model forecasts of tropical cyclones from Australian Monsoon Experiment: Dynamical adjustment of initial conditions. *Meteor. Atmos. Phys.*, **52,** 101–111.

——, 1993b: Eta model forecasts of tropical cyclones from Australian Monsoon Experiment: The model sensitivity. *Meteor. Atmos. Phys.*, **52,** 113–127.

——, and B. Telenta, 1990: Documentation of the UB/NMC (University of Belgrade and National Meteorological Center, Washington) Eta model. Tropical Meteorology Research Programme, WMO, Geneva, WMO/TD-No. 366, 304 pp.

Lilly, D. K., 1962: On the numerical simulation of buoyant convection. *Tellus,* **14,** 148–172.

Liu, W. T., K. B. Katsaros, and J. A. Businger, 1979: Bulk parametrization of air–sea exchanges of heat and water vapor including the molecular constraints at the interface. *J. Atmos. Sci.*, **36,** 1722–1735.

Mangarella, P. A., A. J. Chambers, R. L. Street, and E. Y. Hsu, 1973: Laboratory studies of evaporation and energy transfer through a wavy air–water interface. *J. Phys. Oceanogr.*, **3,** 93–101.

Mellor, G. L., and T. Yamada, 1974: A hierarchy of turbulence closure models for planetary boundary layers. *J. Atmos. Sci.*, **31,** 1791–1806.

——, and ——, 1982: Development of a turbulence closure model for geophysical fluid problems. *Rev. Geophys. Space Phys.*, **20,** 851–875.

Mesinger, F., 1973: A method for construction of second-order accuracy difference schemes permitting no false two-grid-interval wave in the height field. *Tellus,* **25,** 444–458.

——, 1974: An economical explicit scheme which inherently prevents the false two-grid-interval wave in the forecast fields. *Proc. Symp. on Difference and Spectral Methods for Atmosphere and Ocean Dynamics Problems,* Novosibirsk, Russia, Academy of Science, Novosibirsk, 18–34.

——, 1984: A blocking technique for representation of mountains in atmospheric models. *Riv. Meteor. Aeronaut.,* **44,** 195–202.

——, and A. Arakawa, 1976: Numerical methods used in atmospheric models. GARP Publ. Ser., No. 17, Vol. I, WMO, Geneva, 64 pp.

——, and Z. I. Janjić, 1984: Pressure gradient force and hydrostatic equation. Workshop on limited area numerical weather prediction models for computers of limited power, Part I. WMO, programme on short- and medium-range weather prediction research, PSMP Report Series No. 8, 175–234.

——, and ——, 1985: Problems and numerical methods of the incorporation of mountains in atmospheric models. *Large-scale Computations in Fluid Mechanics,* B. E. Engquist, S. Osher, and R. C. J. Somerville, Eds., American Mathematical Society, 81–120.

——, and ——, 1987: Numerical technique for the representation of mountains. *Observation, Theory and Modelling of Orographic Effects, Seminar,* Reading, United Kingdom, ECMWF, 29–80.

——, and T. L. Black, 1989: Verification tests of the eta model, October–November 1988. NOAA/NWS/NMC Washington D.C., Office Note 355, 47 pp.

——, and ——, 1991: Terrain-following vs. a blocking system for the representation of mountains in atmospheric models. *15th IMACS World Congress '91 on Scientific Computation,* Dublin, Intern. Associat. for Mathem. and Computers in Simulation, 575–576.

——, and L. Lobocki, 1991: Sensitivity to the parameterization of surface fluxes in NMC's eta model. *Ninth Conf. on Numerical Weather Prediction,* Denver, CO, Amer. Meteor. Soc., 213–216.

——, ——, S. Ničković, D. Gavrilov, and D. G. Deaven, 1988: The step-mountain coordinate: Model description and performance for cases of Alpine lee cyclogenesis and for a case of Appalachian redevelopment. *Mon. Wea. Rev.,* **116,** 1493–1518.

——, ——, D. W. Plummer, and J. H. Ward, 1990: Eta model precipitation forecasts for a period including Tropical Storm Allison. *Wea. Forecasting,* **3,** 483–493.

Miyakoda, K., and J. Sirutis, 1977: Comparative integrations of global models with various parameterized processes of subgrid-scale vertical transports: Description of the parameterizations. *Contrib. Atmos. Phys.,* **50,** 445–587.

——, and ——, 1983: Impact of sub-grid scale parameterizations on monthly forecasts. *Proc. of the ECMWF Workshop on Convection in Large-scale Models,* Reading, United Kingdom, ECMWF, 231–277.

——, and ——, and J. Ploshay, 1986: One-month forecast experiments-without anomaly boundary forcing. *Mon. Wea. Rev.,* **114,** 2363–2401.

Monin, A. S., and A. M. Obukhov, 1954: Basic laws of turbulent mixing in the surface layer of the atmosphere. *Contrib. Geophys. Inst. Acad. Sci. USSR,* **151,** 163–187 (in Russian).

Phillips, N. A., 1957: A coordinate system having some special advantages for numerical forecasting. *J. Meteor.,* **14,** 184–185.

Rogers, E., G. J. DiMego, and S. J. Lord, 1991: Data assimilation and forecasting for the Tropical Cyclone Motion Experiment (TCM-90) at the National Meteorological Center. *Ninth Conf. on Numerical Weather Prediction,* Denver, CO, Amer. Meteor. Soc., 642–643.

Smagorinsky, J., 1963: General circulation experiments with the primitive equations. Part I: The basic experiment. *Mon. Wea. Rev.,* **91,** 99–164.

Vasiljević, D., 1982: The effect of Mesinger's procedure for preventing grid separation on the geostrophic mode. *Contrib. Atmos. Phys.,* **55,** 177–181.

Ward, J. H., 1990: A review of numerical forecast guidance for hurricane Hugo. *Wea. Forecasting,* **5,** 416–432.

WGNE, 1989: Report of the fourth session of the CAS/JSC Working Group on Numerical Experimentation. WMO, Geneva, No. 4, WMO/TD-No. 278, 76 pp.

——, 1990: Report of the fifth session of the CAS/JSC Working Group on Numerical Experimentation. WMO, Geneva, No. 5, WMO/TD-No. 351.

Xu, Q., 1988: A formula for eddy viscosity in the presence of moist symmetric instability. *J. Atmos. Sci.,* **45,** 5–8.

Zilitinkevitch, S. S., 1970: Dynamics of the planetary boundary layer. *Gidrometeor. Izdat., Leningrad,* 292 pp (in Russian).